

Isolated Ballistic Non-Abelian Interface Channel

Bivas Dutta¹, Vladimir Umansky¹, Mitali Banerjee² and Moty Heiblum^{1,*}

¹*Braun Center for Sub-Micron Research, Department of Condensed Matter Physics,
Weizmann Institute of Science, Rehovot, Israel 76100*

²*Institute of Physics, Faculty of Basic Sciences, École Polytechnique Fédérale de Lausanne,
Lausanne 1015, Switzerland*

* Corresponding author. Email: moty.heiblum@weizmann.ac.il

Non-abelian anyons are prospective candidates for fault-tolerant topological quantum computation due to their long-range entanglement. Curiously these quasiparticles are charge-neutral, hence elusive to most conventional measurement techniques. A proposed host of such quasiparticles is the $\nu=5/2$ quantum Hall state. The gapless edge modes can provide the topological order of the state, which in turn identifies the chirality of the non-abelian mode. Since the $\nu=5/2$ state hosts a variety of edge modes (integer, fractional, neutral), a robust technique is needed to isolate the fractional channel while retaining its original non-abelian character. Moreover, a single non-abelian channel can be easily manipulated to interfere, thus revealing the state's immunity to decoherence. In this work, we exploit a novel approach to gap-out the integer modes of the $\nu=5/2$ state by interfacing the state with integer states, $\nu=2$ & $\nu=3$ ([1](#)). The electrical conductance of the isolated interface channel was $0.5e^2/h$, as expected. More importantly, we find a thermal conductance of $0.5\kappa_0 T$ (with $\kappa_0=\pi^2k_B^2/3h$), confirming unambiguously the non-abelian nature of the $\nu=1/2$ interface channel and its Particle-Hole Pfaffian topological order. Our result opens new avenues to manipulate and test other exotic QHE states and braid, via interference, the isolated fractional channels.

The fractional quantum Hall effect (FQHE) harbors fractionally charged quasiparticles localized in the 2D bulk surrounded by conducting chiral edge modes at the periphery([2](#)). Laughlin's states and their 'particle-hole conjugated' states are abelian([2](#)). In higher Landau levels, exotic non-abelian states are expected, each with a highly degenerate ground-state([3, 4](#)). A proposed state that hosts such exotic quasiparticles is the $\nu=5/2$ state, with gapless edge-modes: two integer modes ($\nu=2$), a fractional mode ($\nu=1/2$), and neutral Majorana modes (their number and chirality depend on the state's topological order). To capture the nature of the state, we recently employed thermal conductance G_{th} measurement([5](#)), which is sensitive to all energy-carrying modes (charged and neutral alike). The measured G_{th} is a vital topological invariant that dictates the state's topological order when all edge modes are fully thermal-equilibrated.

In the abelian regime, with fully equilibrated downstream (DS) and upstream (US) modes, the thermal conductance is given by $G_{\text{th}}=(n_d - n_u)\kappa_0T$, with $\kappa_0 = \pi^2k_B^2/3h$ the quantum of thermal conductance, k_B the Boltzmann's constant, h the Planck's constant, T the temperature, and n_d (n_u) is the number of downstream (upstream) edge modes. However, in the absence of thermal equilibration, one expects $G_{\text{th}}= (n_d + n_u)\kappa_0T$ (6). In the non-abelian regime G_{th} comes with fractional multiples of κ_0T , originating from the fractional nature of the chiral central charge(7). With this ambiguity in mind, we found experimentally $K_{5/2}=2.5\kappa_0$ (5), suggesting the Particle-Hole Pfaffian (PH-Pf) topological order of the state, disagreeing with the numerical calculations(8-23). However, the nature of the *isolated* Majorana edge mode, tied with the $\nu=1/2$ charge mode, was never confirmed.

Here, we demonstrate the employment of a method we used to separate the fractional mode from its integer companions(1). Our realization exploited an interface between two adjacent quantum Hall states(1), with an *isolated channel* emerging at the interface. In particular, the interface between the $\nu=5/2$ state and the gate-defined $\nu=2$ or $\nu=3$, leads to a chiral or an anti-chiral $\nu=1/2$ interface modes. We found a thermal conductance coefficient of the isolated channel to be $K_{1/2}=0.5\kappa_0$ – indicating the non-abelian nature of the isolated channel, with its topological order agreeing with the PH-Pf(5).

Molecular Beam Epitaxy (MBE) grown high quality GaAs-AlGaAs heterostructures with shallow-DX-centers doping(24), allowing 'hysteresis free' gating and negligible heat conductance of the bulk at millikelvin temperatures(1). This particular doping leads to higher disorder in comparison to the conventional superlattice (SPSL) doping technique(5, 24, 25). Our experimental setup, with the 'heart' of the fabricated two-arm device is shown in Fig. 1A. The inner gates (yellow) and the outer ones (violet) tune the filling factor of each of the two bulks. The gates are separated from the sample by about a 25nm thick HfO_2 layer (for more details, see SM Sec. II). Gate voltage in the range $-1.5\text{V}<V_g<+0.3\text{V}$ allows varying the electron density from pinch-off to $3\times 10^{11}\text{cm}^{-2}$ (see Fig. S1); thus controlling the filling factor. The resulting interface modes split when leaving the small floating ohmic contact ($20\times 2\mu\text{m}^2$, shown in red), which connects the two arms. This contact serves as a heated reservoir. Large ohmic contacts (S, D, G, shown in cyan) are placed at the interfaces, while separate contacts, located at the physical edge of the mesa (not shown), probe the filling factor of each of the respective bulks.

Current I_S is injected from S and dissipates power $\Delta P = \frac{1}{4}I_S^2R_S$ in the floating contact (R_S the two-terminal resistance of the interface). Figure 1B provides a schematic representation of the heat balance in the floating contact at the interface. Heat leaving the floating contact is composed of a phononic contribution $\Delta P_{ph}=\beta(T_m^5 - T_0^5)$ and an electronic contribution $\Delta P_e = 0.5K(T_m^2 - T_0^2)$, where T_m is the temperature of the floating contact and T_0 the base temperature, with $\Delta P = \Delta P_{ph} + \Delta P_e$ at equilibrium.

For our small floating reservoir, the phononic contribution is negligible at $T_m < 20\text{mK}$. The temperature T_m is determined by measuring the ‘low frequency’ Johnson-Nyquist (J-N) thermal noise at the drain contact D , which is placed about $160\mu\text{m}$ away along downstream in one arm (see [SM Sec. III](#)). The noise is filtered by an LC resonant circuit (resonance frequency 630 kHz and bandwidth 10-30kHz), amplified by a low-noise cold voltage pre-amplifier (placed on the 4.2K plate), followed by a room-temperature amplifier.

In general, our experimental strategy is to tune the inner regions to the ‘tested’ state ν_{in} (e.g., $5/2$), and the outer regions to an integer state ν_{out} (e.g., 0, 1, 2, 3); leading to an ‘interface filling’ $\nu_{int} = \nu_{in} - \nu_{out}$ (with the nomenclature ‘ $\nu_{in} - \nu_{out}$ ’, used in all figures). The chirality of the interface charge mode reverses when the interfacing condition changes from $\nu_{in} > \nu_{out}$ to $\nu_{in} < \nu_{out}$. Having a single amplifier located downstream, the magnetic field was reversed between these two cases (see [SM Sec. III](#)).

We start with measurements of interface modes formed in the configurations ‘3-2’, ‘3-1’ and ‘3-0’. The two-probe source resistance R_s exhibits quantized plateaus as a function of the gate voltage, h/e^2 , $h/2e^2$, and $h/3e^2$ ($\sim 0.1\%$ accuracy), with the expected thermal conductances $1\kappa_0 T$, $2\kappa_0 T$, and $3\kappa_0 T$, respectively ([26](#), [27](#)). In these chiral configurations, the downstream modes are equilibrated right from the start at the reservoir temperature T_m , which is determined by measuring the thermal J-N noise (S_{th}) at the drain (See [SM Sec. III](#)). The J-N noise and the deduced T_m are plotted in [Figs. 2A & 2B](#). We analyze the data in two ways: *i*. By fitting the linear-electronic contribution, ΔP versus T_m^2 for $T_m < 18\text{mK}$, and find $K \cong 1\kappa_0$, $2\kappa_0$, and $3\kappa_0$, respectively ([Fig. 2C](#)); *ii*. By fitting the data for $T_m < 30\text{mK}$ ([Fig. 2D](#)), which reflects the electronic and phononic contributions. A similar quantization of the thermal conductance is found with $\beta \approx 5 \times 10^9 \text{WK}^{-5}$ ([5](#)).

Interfacing $\nu=7/3$, $5/2$, and $8/3$ with $\nu=2$ and $\nu=3$, leads to a source resistance shown in [Fig. 3A](#). Well-quantized plateaus indicate full charge equilibration at the interfaces. We start with the $\nu=7/3$ and $8/3$ abelian states. Interfacing these two states with $\nu=2$ results in an effective modes’ filling of $\nu=1/3$ for ‘7/3-2’ interface and $\nu=2/3$ mode for ‘8/3-2’ interface (the latter is accompanied by an upstream neutral mode). The interface chirality is reversed when these states are interfaced with $\nu=3$: the $\nu=2/3$ charge mode accompanied by a neutral mode appears for ‘7/3-3’ interface and a single $\nu=1/3$ charge mode appears for the ‘8/3-3’ interface. The measured two-terminal thermal conductances in these four cases are shown in [Figs. 3B & 3C](#). The results agree with good accuracy with the theoretical expectations ([5](#)).

The $\nu=5/2$ state may host different topological orders, with each having different modes structure and a different thermal conductance ([28](#)). Here, we consider the two competing candidates: Particle-Hole-Pfaffian (PH-Pf) and Anti-Pfaffian (A-Pf). For a discussion of other possible orders, see [SM Sec. VI](#). Both orders support counterpropagating modes at the bare edge of the sample or, equivalently, the ‘5/2-0’

configuration (Figs. 4A-4B). Aside from two downstream integer charge modes and a $\nu=1/2$ charge mode, the PH-Pf order supports an upstream Majorana mode, while in comparison, the A-Pf order supports three upstream Majorana modes (two Majorana modes form a single bosonic neutral mode). With counterpropagating modes, an accurate determination of the thermal equilibration between all modes is imperative. With a full (none) thermal equilibration, one expects thermal conductance $2.5\kappa_0T$ ($3.5\kappa_0T$) for the PH-Pf and $1.5\kappa_0T$ ($4.5\kappa_0T$) for A-Pf.

Figures 4A-4F present different configurations: '5/2-0', '5/2-1', '5/2-2'. As shown in the figures, the expected two-terminal thermal conductance of the PH-Pf and A-Pf may overlap considering the range from full thermal equilibration to no equilibration. However, the interface '5/2-3' allows a clear distinction between the two topological orders (Fig. 4G-4H). Here, the interface channel for the A-Pf order supports two co-propagating modes, both leaving the hot reservoir at temperature T_m (hence, equilibrated) with an expected thermal conductance $1.5\kappa_0T$. By contrast, the PH-Pf order supports an interface channel with counterpropagating charge and a Majorana mode, leading to thermal conductance in the range $0.5\kappa_0T - 1.5\kappa_0T$.

In Figs. 4I-4L, we present the measurement results of ΔP vs T_m^2 for the four 5/2-interfaces: '5/2-0', '5/2-1', '5/2-2' and '5/2-3'. The measured thermal conductances are $(2.55\pm 0.07)\kappa_0T$, $(1.53\pm 0.04)\kappa_0T$, $(0.55\pm 0.02)\kappa_0T$, and $(0.53\pm 0.02)\kappa_0T$, respectively. These results, especially for the decisive-'5/2-3' interface, rules out the A-Pf order and point at the fully equilibrated PH-Pf order (Figs. 4A-4H). Above all, the observed $1/2$ -quanta thermal conductance of the fully equilibrated-isolated interface $\nu=1/2$ and Majorana channel, proves unambiguously its non-abelian nature.

The $\nu=5/2$ state has been attracting a wide spread attention due to growing expectations of realizing non-abelian anyons in condensed matter systems. But only proving the presence of non-abelian character of the state is not enough unless there is a robust sustainable method that allows isolating the non-abelian part from the trivial ones. Our work exploits a novel '*interfacing*' method (1), which allows measuring the thermal conductance of the emergent 'interface channel' at the junction between two adjacent QHE states; the 5/2 state and the integer states 2 and 3. The advantage of the interfacing method lies in the elimination of the integer modes and thus allowing a direct measurement of the isolated non-abelian interface channel. Moreover, this method allows a clear distinction between competing orders of the $\nu=5/2$ state. This configuration can be readily applied for interfering the singled-out non-abelian channel, thus allowing for the braiding operations - a necessary step in topological quantum processing.

References

1. B. Dutta *et al.*, Novel method distinguishing between competing topological orders. *Accepted in Science (2021)*, *arXiv preprint arXiv:2101.01419*, (2021).
2. M. Heiblum, D. E. Feldman, Edge probes of topological order. *International Journal of Modern Physics A* **35**, (2020).
3. X. G. Wen, Non-Abelian statistics in the fractional quantum Hall states. *Physical Review Letters* **66**, 802-805 (1991).
4. J. B. Pendry, Quantum limits to the flow of Information and entropy. *Journal of Physics a-Mathematical and General* **16**, 2161-2171 (1983).
5. M. Banerjee *et al.*, Observation of half-integer thermal Hall conductance. *Nature* **559**, 205-210 (2018).
6. C. L. Kane, M. P. A. Fisher, Quantized thermal transport in the fractional quantum Hall effect. *Physical Review B* **55**, 15832-15837 (1997).
7. A. Gromov, G. Y. Cho, Y. You, A. G. Abanov, E. Fradkin, Framing Anomaly in the Effective Theory of the Fractional Quantum Hall Effect. *Physical Review Letters* **114**, 016805 (2015).
8. R. H. Morf, Transition from quantum Hall to compressible states in the second Landau Level: new light on the $\nu=5/2$ enigma. *Physical Review Letters* **80**, 1505-1508 (1998).
9. M. Storni, R. H. Morf, S. Das Sarma, Fractional quantum Hall state at $\nu=5/2$ and the Moore-Read pfaffian. *Physical Review Letters* **104**, 076803 (2010).
10. G. Moore, N. Read, Nonabelions in the fractional quantum Hall effect. *Nuclear Physics B* **360**, 362-396 (1991).
11. M. Levin, B. I. Halperin, B. Rosenow, Particle-Hole Symmetry and the Pfaffian State. *Physical Review Letters* **99**, 236806 (2007).
12. S. S. Lee, S. Ryu, C. Nayak, M. P. Fisher, Particle-hole symmetry and the $\nu = 5/2$ quantum Hall state. *Physical Review Letters* **99**, 236807 (2007).
13. M. P. Zaletel, R. S. K. Mong, F. Pollmann, E. H. Rezayi, Infinite density matrix renormalization group for multicomponent quantum Hall systems. *Physical Review B* **91**, 12 (2015).
14. E. H. Rezayi, Landau Level mixing and the ground state of the $\nu=5/2$ quantum Hall effect. *Physical Review Letters* **119**, 026801 (2017).
15. P. T. Zucker, D. E. Feldman, Stabilization of the particle-hole pfaffian order by Landau-Level mixing and impurities that break particle-hole symmetry. *Physical Review Letters* **117**, 096802 (2016).
16. D. F. Mross, Y. Oreg, A. Stern, G. Margalit, M. Heiblum, Theory of disorder-induced half-integer thermal Hall conductance. *Physical Review Letters* **121**, 026801 (2018).

17. C. Wang, A. Vishwanath, B. I. Halperin, Topological order from disorder and the quantized Hall thermal metal: Possible applications to the $\nu=5/2$ state. *Physical Review B* **98**, 045112 (2018).
18. I. C. Fulga, Y. Oreg, A. D. Mirlin, A. Stern, D. F. Mross, Temperature Enhancement of Thermal Hall Conductance Quantization. *Physical Review Letters* **125**, 236802 (2020).
19. B. Lian, J. Wang, Theory of the disordered $\nu=5/2$ quantum thermal Hall state: Emergent symmetry and phase diagram. *Physical Review B* **97**, (2018).
20. S. H. Simon, Interpretation of thermal conductance of the $\nu = 5/2$ edge. *Physical Review B* **97**, 121406 (2018).
21. D. E. Feldman, Comment on "Interpretation of thermal conductance of the $\nu=5/2$ edge". *Physical Review B* **98**, 167401 (2018).
22. S. H. Simon, B. Rosenow, Partial Equilibration of the Anti-Pfaffian Edge due to Majorana Disorder. *Physical Review Letters* **124**, 126801 (2020).
23. K. K. W. Ma, D. E. Feldman, Thermal Equilibration on the Edges of Topological Liquids. *Physical Review Letters* **125**, (2020).
24. V. Umansky, M. Heiblum, *MBE growth of high-mobility 2DEG*. M. Henini, Ed., Molecular Beam Epitaxy: From Research to Mass Production (Elsevier Science BV, Netherlands, 2013), pp. 121-137.
25. K. A. V. Rosales *et al.*, Fractional Quantum Hall Effect Energy Gaps: Role of Electron Layer Thickness. *Physical Review Letters* **127**, (2021).
26. M. Banerjee *et al.*, Observed quantization of anyonic heat flow. *Nature* **545**, 75-79 (2017).
27. S. Jezouin *et al.*, Quantum limit of heat flow across a single electronic channel. *Science* **342**, 601-604 (2013).
28. K. K. W. Ma, D. E. Feldman, The sixteenfold way and the quantum Hall effect at half-integer filling factors. *Phys. Rev. B* **100**, 035302 (2019).
29. M. O. Goerbig, P. Lederer, C. Morais Smith, Microscopic theory of the reentrant integer quantum Hall effect in the first and second excited Landau levels. *Physical Review B* **68**, 241302 (2003).

Acknowledgments

We acknowledge D. Mross for a critical reading of the manuscript, followed by useful suggestions. B.D. acknowledges the support from Clore Foundation. M.H. acknowledges the continuous support of the Sub-Micron Center staff, the support of the European Research Council under the European Community's Seventh Framework Program (FP7/2007-2013)/ERC under grant agreement number 713351, the partial support of the Minerva foundation under grant number 713534.

Author contributions

B.D., M.H. designed the experiment, B.D. fabricated the devices and performed the measurements and did the analysis. B.D, M.B, and M.H participated in discussions and presenting the data. V. U. developed and grew the heterostructures supporting the 2DEG. All authors contributed to the manuscript writing.

Competing interests

The authors declare no competing interests.

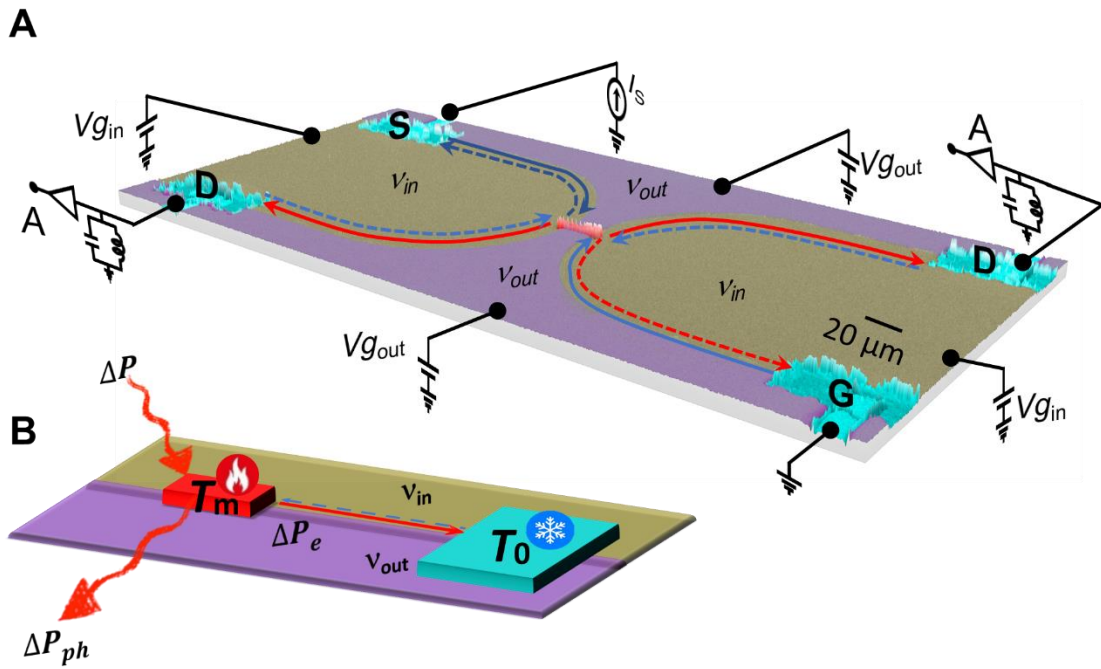


Figure 1 | The experimental setup used to measure the interface thermal conductance. (A) False colored SEM micrograph of the heart of the device. Two biased top gates, inner-gate ($V_{g_{in}}$, yellow) and outer-gate ($V_{g_{out}}$, violet), divide the 2DEG mesa into two gate-defined arms. A small floating ohmic contact (red, dimensions $20 \times 2 \mu\text{m}^2$) connects the two arms. Large contacts (S, D, G, in cyan) probe the interface filling. Added ohmic contacts at the edge of MESA (not shown here) probe the filling of the respective sides. The floating contact is heated to T_m by an injecting current I_s from S. Its temperature is determined by measuring the low-frequency Johnson-Nyquist noise at 630kHz (LC bandwidth 10-30kHz), after amplification by a cooled pre-amplifier (at 4.2K) followed by a room-temperature amplifier. Arrows indicate the interface-modes at '5/2-3' interface as an example (see Fig. 4). **(B)** Schematic representation of heat balance in the floating contact, with the same color-codes as in A, showing only a zoomed-in part of the interface along downstream. An injected current dissipates power ΔP , which is evacuated by two main channels: the phononic channel ΔP_{ph} and the electronic channel ΔP_e . The cold reservoir contact G is at temperature T_0 . Due to the small volume of the floating contact, the phononic contribution is negligible at low temperatures.

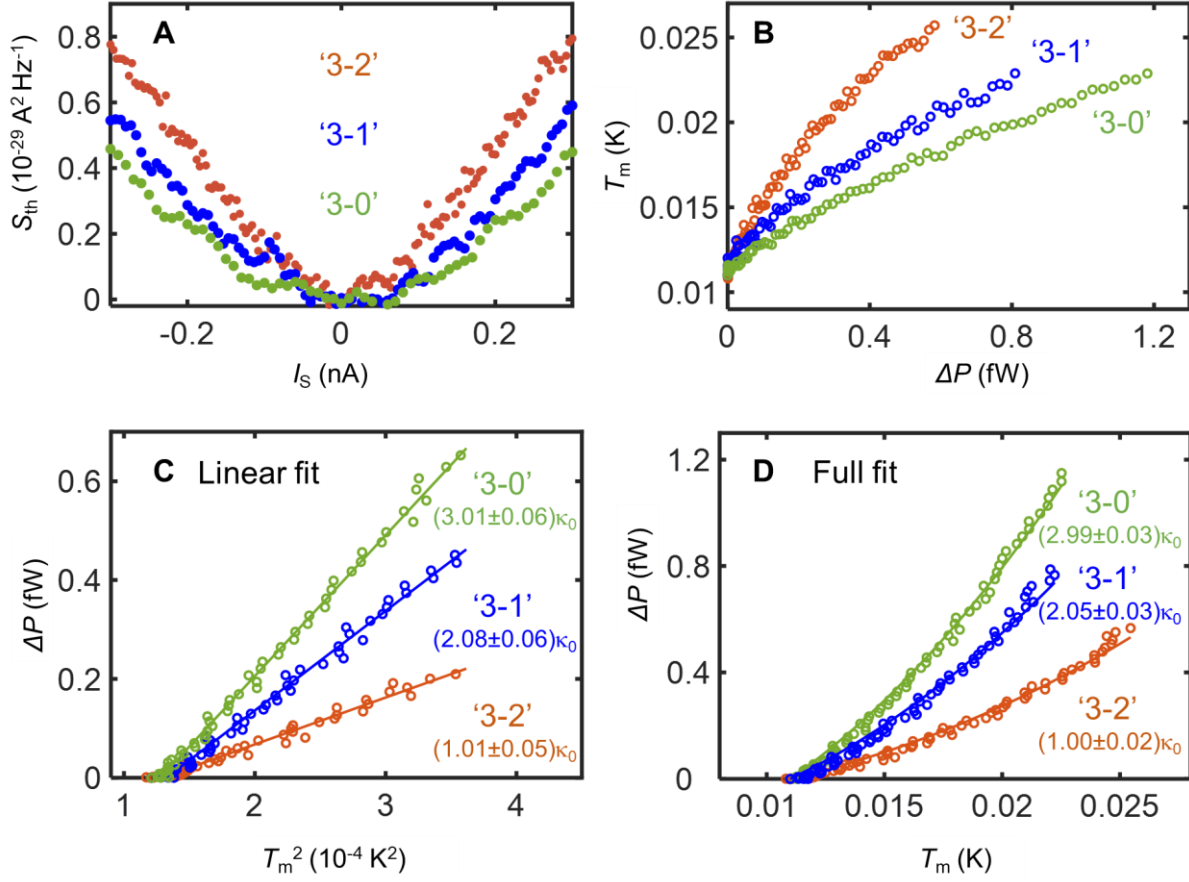


Figure 2 | Noise, temperature, and dissipation at integer interfaces. (A) Excess Johnson-Nyquist noise S_{th} as function with heating current I_s for the three ‘integer interfaces’: ‘3-2’ (orange), ‘3-1’ (blue), and ‘3-0’ (green) at $T_0=11\text{mK}$. **(B)** Calculated temperature T_m as a function of the dissipated power $\Delta P = 0.25I_s^2R_S$, with R_S the ‘interface mode’ resistance, for the three different configurations (see SM Sec. V). **(C)** Dissipated power as a function of squared temperature in the range $T_m < 18\text{mK}$. The thermal conductance is determined from the slope, via $\Delta P = \frac{1}{2}K(T_m^2 - T_0^2)$. **(D)** Dissipated power as a function of temperature in the range $T_m < 30\text{mK}$. Here, phonon contribution is included, via $\Delta P = \frac{1}{2}\kappa(T_m^2 - T_0^2) + \beta(T_m^5 - T_0^5)$, with e-ph coupling constant $\beta \approx 5 \times 10^9 \text{ WK}^{-5}$.

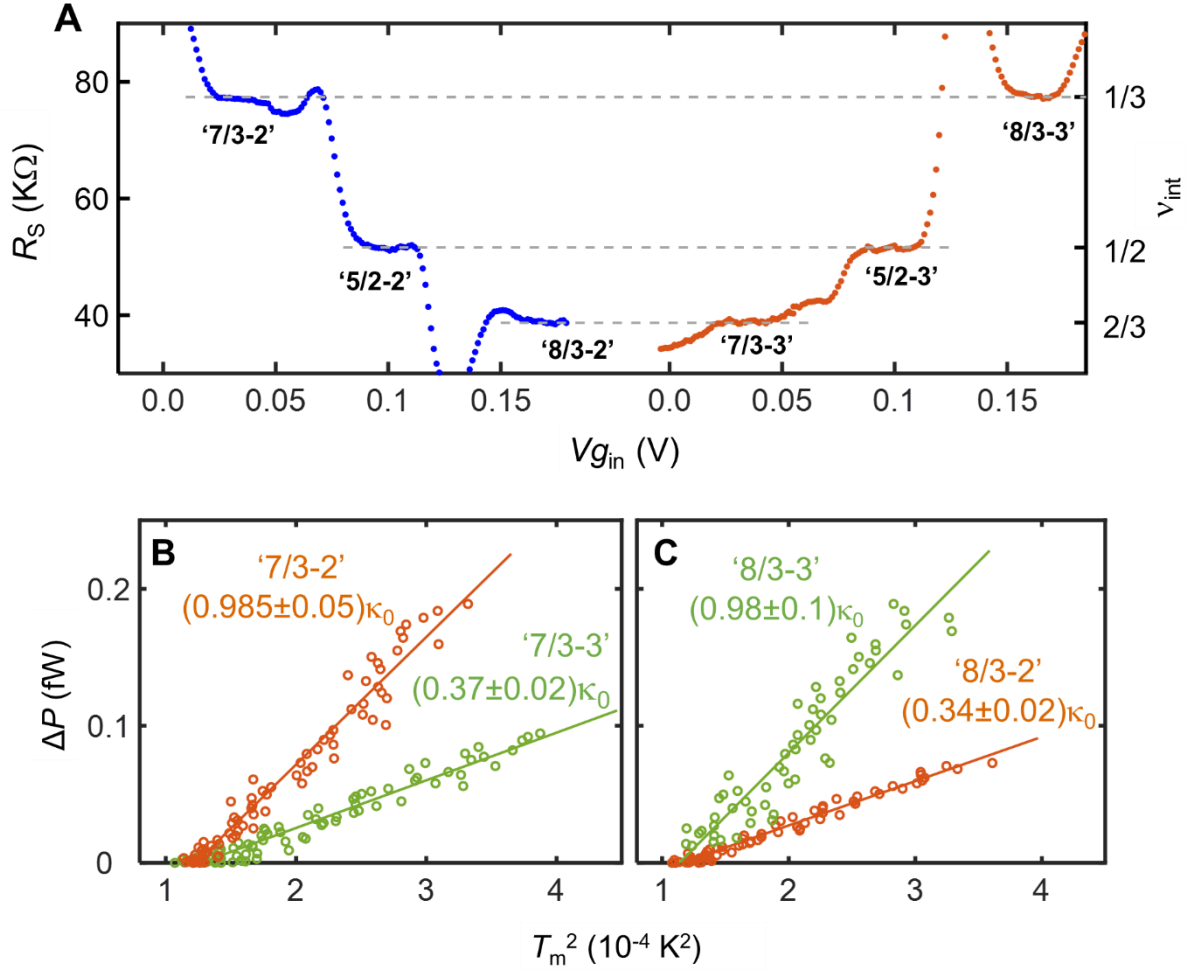


Figure 3 | Interface resistance and thermal conductance of states in the 2nd LL. (A) Two terminal source interface resistance of ‘7/3-2&3’, ‘5/2-2&3’, and ‘8/3-2&3’. Quantized plateaus indicate full charge equilibration at the interface. The peaks and dips are attributed to reentrant effects(29). **(B)** Determination of the thermal conductance for $T_m < 18\text{mK}$, as was done in Fig. 2. The slope for ‘7/3-2’ is close to unity, as expected for the 1/3 interface mode. The slope for ‘7/3-3’ is $0.37\kappa_0$, and not zero - due to the well-known lack of equilibration of the resultant 2/3 mode(26). **(C)** Similar data as in B, at different interfacing conditions with $\nu=8/3$.

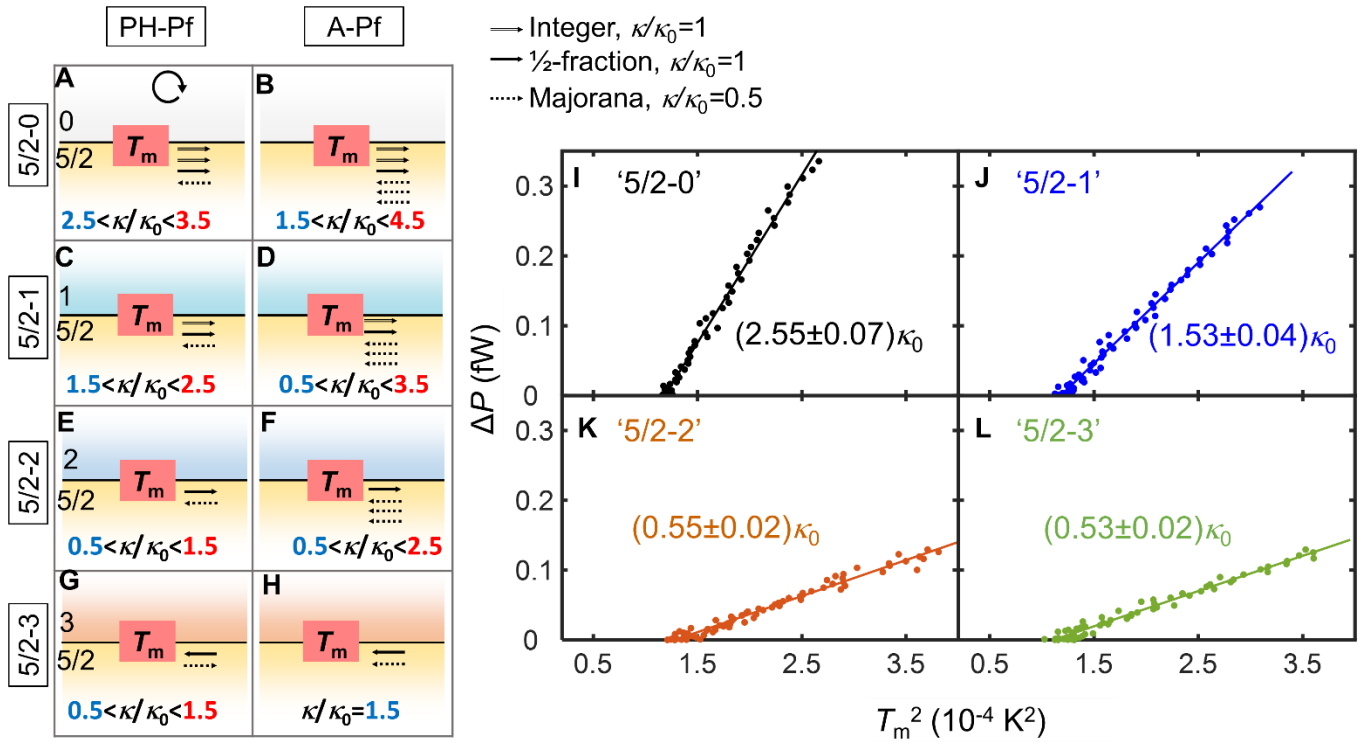


Figure 4 | Thermal conductance of the '5/2-n' interfaces. (A-H) Plotted are the interface modes of the interfaced PH-Pf and the A-Pf orders with different integers, and the expected thermal conductance in each case. Fully-equilibrated value in light-blue and un-equilibrated value in red. Notation of the arrows are indicated in the inset. Clockwise chirality is indicated by the circled arrow. **(I-L)** Plots of the dissipated power as a function of the squared temperature with linear fits as in Figs. 2 & 3, for all four 5/2-interfaces. The extracted thermal conductance values, in particular for '5/2-3', unambiguously exclude the A-Pf topological order (see G-H), and agrees (with small estimated errors) with the Ph-Pf topological order.

Supplementary Materials: Isolated Ballistic Non-Abelian Interface Channel

Bivas Dutta¹, Vladimir Umansky¹, Mitali Banerjee² and Moty Heiblum^{1,*}

¹*Braun Center for Sub-Micron Research, Department of Condensed Matter Physics,
Weizmann Institute of Science, Rehovot, Israel 76100*

²*Institute of Physics, Faculty of Basic Sciences, École Polytechnique Fédérale de Lausanne,
Lausanne 1015 Switzerland*

* Corresponding author. Email: moty.heiblum@weizmann.ac.il

I. MBE-grown ‘inverted’ heterostructure

The heterostructures used in these experiments were designed to achieve a compromise between the robustness of the 5/2 fractional state and the ability to operate it with surface gates. It is well established that a quantization of the 5/2 state is governed by the long-range spatial potential landscape formed by the ionized donors. Smoothing this landscape is customarily achieved by excessive doping, either in ‘short period superlattice’[\(24\)](#), or in a low Al-mole-fraction in AlGaAs[\(5\)](#). These doping schemes provide a significant reduction in the long-range potential fluctuations via spatial correlations between ionized donors, exhibiting, at the same time, negligible lateral parasitic conductance at low temperatures. Unfortunately, weakly localized electrons in such doped layers both thwart the stable operation of the surface gates and completely inhibit applying positive gate bias, which is essential in the present experiment. In order to solve the problem, we use the so-called ‘inverted’ 2DEG structure, where an accurate quantization of the 5/2 state is enabled by excess δ -doping in a layer of $\text{Al}_x\text{Ga}_{1-x}\text{As}$ ($x=0.23$) placed 60nm below the QW (see [Fig. S1](#)). The surface potential is compensated using a uniformly doped layer made of $\text{Al}_{0.37}\text{Ga}_{0.63}\text{As}:\text{Si}$, located far away from the QW, thus minimizing the impact of its long-range random potential fluctuations on the 2DEG. Such high Al mole-fraction doped layers are conventionally used between the gates and the 2DEG in most devices since the electrons freeze at $T \sim 100\text{K}$ in the DX-Si centers. The electron density in as-grown samples at 300mK is $\sim 2.4 \times 10^{11} \text{cm}^{-2}$ and the mobility is about $15 \times 10^6 \text{cm}^2/\text{Vs}$, even though the 2DEG wavefunction is asymmetrically shifted towards the bottom AlGaAs-GaAs interface - usually considered to be of lower quality than the top interface of the quantum well.

II. Device fabrication

We start with a 250x800 μm MESA, made by wet etching in $\text{H}_2\text{O}_2:\text{H}_3\text{PO}_4:\text{H}_2\text{O}=1:1:50$ solution for 2 mins resulting with etched depth of about 180 nm. In the next step, a few ohmic contacts are patterned by e-beam-lithography at the edge and in the bulk of the MESA, followed forming the ohmic contacts by metal deposition (with standard material ratio $\text{Au}:\text{Ge}:\text{Ni} = 2:1:0.75$), followed by annealing at 450 $^\circ\text{C}$ for 2 mins. Some of the contacts are shown in Fig. 1a as S, G, D contacts. The whole sample is then coated with 25 nm of HfO_2 layer via ALD, acting as dielectric medium for the metallic-gate that follows. In the next step, the outer-gate ($V_{g_{\text{out}}}$) is patterned by e-beam-lithography and subsequently deposited a 20 nm Ti/Au thin metallic film, acting as the outer-gate. We then coat the sample with another 15 nm thick of HfO_2 layer, which separates the outer-gate from the following inner-gate. Next step consist of patterning of inner-gate ($V_{g_{\text{in}}}$) and subsequent metallization by 20 nm Ti/Au thin film. The ohmic contacts (such as S, G, D) in the bulk of the MESA were designed such that they sit exactly at the interface of the two gates. In the final step, the interface-ohmic contacts (like, S, D, G contacts) are connected to the bonding-pads by thick gold lines, passing over the HfO_2 covered outer-gate, such that they do not short to the gates.

III. Experimental setup

The heart of the device is shown in Fig. 1a. Gate voltages ($V_{g_{\text{in}}}$ and $V_{g_{\text{out}}}$) are applied to divide the mesa into two gate-defined arms. The small-floating ohmic contact with area $20 \times 2 \mu\text{m}^2$ act as the floating hot-reservoir connecting the two arms. An injected DC current I_s from the interface-contact 'S' heats up the floating contact to temperature T_m . The voltage amplifiers are connected to the drain contact 'D' at the interface. Thermal voltage fluctuations (S_v) of the hot-floating contact is measured by the amplifiers after being filtered by the LC resonant circuit. The voltage fluctuations are converted into current fluctuations as $S_{\text{th}} = S_v G_{\text{int}}^2$, with G_{int} the conductance of the interface mode.

In the following we give an example, which describes the experimental process for the measurements at the 5/2-interfaces. First, the magnetic field is tuned to a value $B \approx (-/+)$ 4T (chirality clockwise/anti-clockwise). At this magnetic field, with the bare density ($n \sim 2.4 \times 10^{11} \text{cm}^{-2}$) the whole sample remains at a filling $\nu > 2$, just outside the $\text{ff}=2$ plateau. Now, we create 5/2-interfaces by tuning the gates. For making '5/2-n' interface, where, $n=2,1,0$ (at $B=-4\text{T}$), we apply positive gate voltage $V_{g_{\text{in}}}$ to populate the inner-gated region to $\nu_{\text{in}}=5/2$, while apply a negative gate voltage $V_{g_{\text{out}}}$ on the outer-gate to deplete the outer-gated region to $\nu_{\text{out}}=2, 1$, or fully pinch to $\nu_{\text{out}}=0$. Similarly, for making '5/2-3' interface (at $B=+4\text{T}$; with a fixed amplifier position we needed to reverse B to +4T, to have the amplifier on the downstream side), we apply

certain positive gate voltages on both gates to populate the inner-gated regions to $\nu_{in}=5/2$, and the outer-gated region to $\nu_{out}=3$, respectively. Secondly, to characterize the ‘interface-mode’, we measure the 2-terminal resistance at the interface ohmic contacts (e.g., at ‘S’). Nicely quantized interface-resistance ensures proper charge equilibration. Next, we measure the branching of the impinging current at the floating Ohmic contact. We assure symmetric partitions of the current between the two arms, with less than 2% reflections. After this, we proceed for the thermal conductance measurements at the interface.

IV. Determination of amplifier Gain and T_0

The gain of the amplifier is a crucial parameter to determine the temperature T_m of the floating-contact. We take the advantage of the temperature dependent Johnson-Nyquist voltage noise of the well-known Hall-resistance R_S of the interface modes to calibrate the gain of amplifier. The equilibrium voltage noise of the R_S (well-known with good accuracy) is measured at the central frequency ($f_0 \sim 630\text{KHz}$) of the LC resonant circuit, with a Δf bandwidth opened at the spectrum analyzer, for different cryostat (bath) temperatures T_{bath} measured by well calibrated commercial thermometers, $S_V = 4k_B R_S T_{bath} G_h^2 G_c^2 \Delta f + S_{const}$, where k_B , the Boltzmann constant; $G_h=400$, the known gain of the room-temperature amplifier; and S_{const} is the temperature independent voltage noise of the amplifier. A plot of the normalized voltage noise, $S_{norm} = S_V / (4k_B R_S G_h \Delta f)$, at the ‘2-1’ interface, with different bath temperatures is shown in Fig. S2. The slope of the linear fit of the data gives the gain of the cold amplifier, $G_c = \sqrt{\Delta S_{norm} / \Delta T}$. The obtained gain at this interface is $G_c \sim 7.7$, which is the effective gain of the amplifier depending on the particular bandwidth of the LC circuit. For different interface modes the bandwidth (depends on R_S) of the circuit changes and so the effective gain of the amplifier. The ratio of the areas of resonance curves for two interfaces is directly proportional to the ratio of the squared gains in the two cases. The area under the LC resonance curves for two interfaces (with two different R_S) were compared to extract the gain at different interface fillings. After knowing the gain of the amplifier, the temperature T_0 is inferred from the above calibration curve, by measuring the thermal-background noise of the interface resistances.

V. Determination of T_m

We extract the temperature T_m of the small-floating contact by measuring the excess thermal fluctuations from the floating contact carried out by the interface edge modes. Using the general expression for the

excess current noise S_{th} , carried out by n_1 and n_2 number edge channels in the two arms, we get the temperature of the floating contact T_m given by,

$$T_m = T_0 + S_{th}/2k_B G^*,$$

Where, $G^* = G_{int} \frac{n_2(n-n_2)}{n}$, with $n = n_1 + n_2$, and G_{int} is the conductance of the interface mode. In our case $n_1 = n_2$, therefore, $G^* = \frac{1}{2} G_{int}$.

VI. 5/2-interface thermal conductance for other possible topological orders

In the main text we have considered PH-Pf and A-Pf topological orders of $\nu=5/2$ state. The Pf order (Fig. S3), which supports a DS Majorana mode, is also numerically favorable. But the observation of US noise makes it experimentally unlikely. Still, at the interface of the Pf-order with $\nu=2$ (Fig. S3) one expects a definite value of thermal conductance $KT=1.5\kappa_0 T$, which doesn't match the observed value in our experiment, $KT \cong 0.5\kappa_0 T$ (see Fig. 4K). Therefore, we can exclude the Pf order. Similarly all other a-priori possible topological orders can be excluded either by the interface with $\nu=2$ or with $\nu=3$ (28).

VII. Hall measurements near $\nu=5/2$ state

Fig. S4 shows the 2-probe Hall resistance R_{xy} with magnetic field B near the $\nu=5/2$ state, measured at the physical edge of sample (with $\nu=0$ outside), showing a well quantized plateau.

VIII. 5/2-interface thermal conductance with small variation of filling on the plateau and the base temperature T_0

The Fig. S5-S6 shows the data for the thermal conductance at the interface '5/2-3' with different filling factors ν_{in} around $\nu=5/2$ and at different base temperature T_0 . The measured values found to be more or less constant with the changes of filling factors and temperatures, with $\kappa \approx 0.5\kappa_0$.

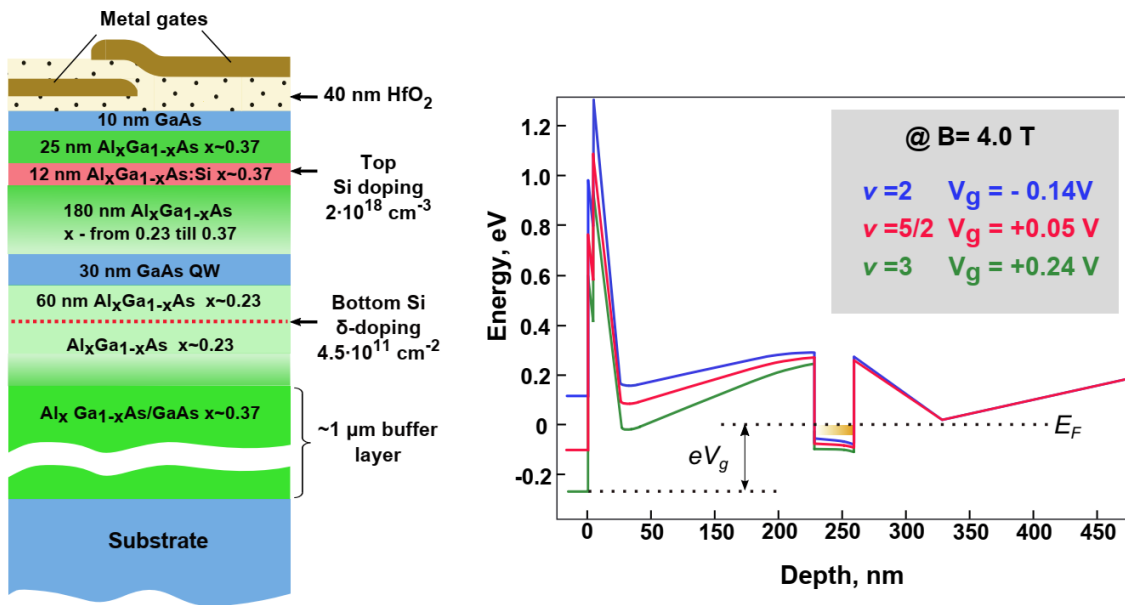


Figure S1 | MBE growth structure of the heterostructure. **left**, Cross-section of the MBE growth (not in scale). **right**, Conduction band at three different gate voltages corresponding to three different filling factors $\nu=2, 5/2,$ and 3 .

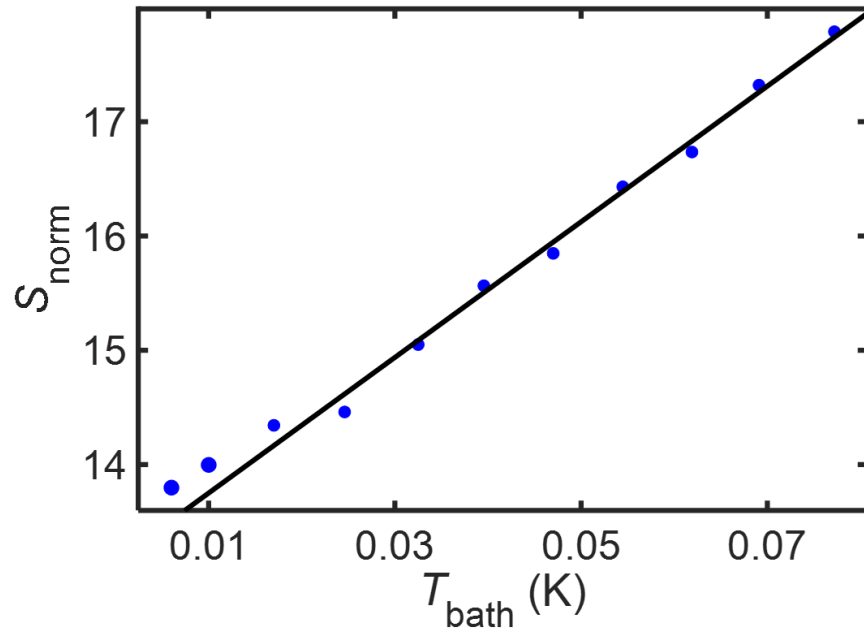


Figure S2 | Calibration of the amplifier. Temperature-dependent Johnson-Nyquist noise of the interface resistance R_S allows calibration of the amplifier. The normalized noise at the '2-1' interface is plotted with the bath temperature. The slope of the linear fit gives the gain of the amplifier for this interface.

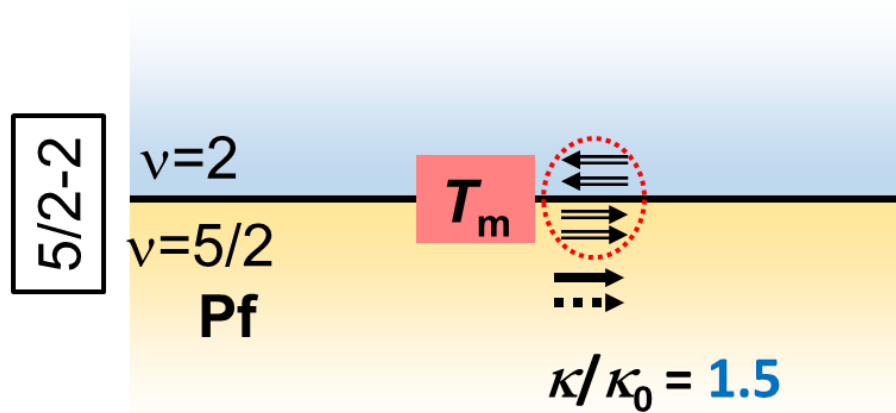


Figure S3 | expected interface thermal conductance for '5/2-2' interface with the Pf topological order. At the interface of $\nu=5/2$ -Pf order with $\nu=2$, two integer modes are gapped out, leaving at the interface $\nu=1/2$ and a Majorana mode both in the DS, hence, thermally equilibrated at T_m . The expected thermal conductance is $1.5\kappa_0 T$, in disagreement with the experimentally observed value (Fig. 4k).

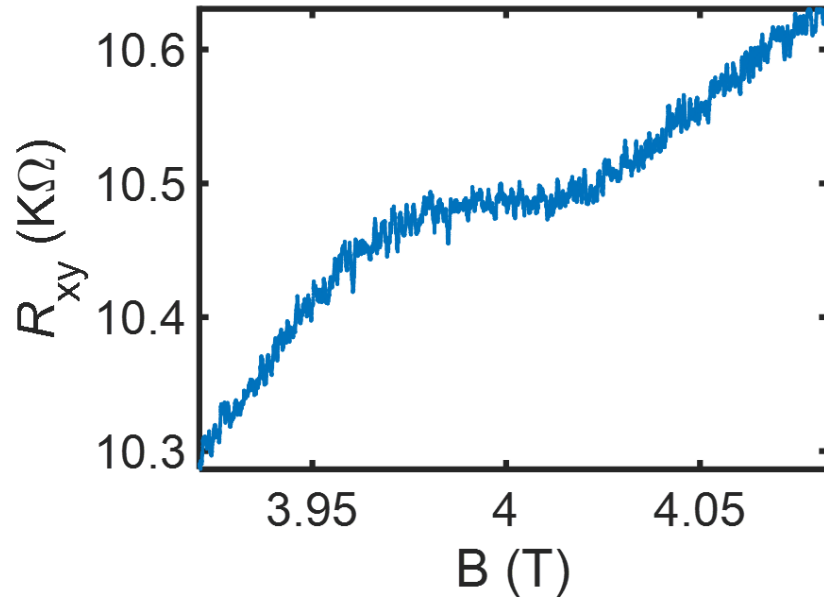


Figure S4| Hall measurements near $\nu=5/2$. 2-probe Hall resistance R_{xy} with magnetic field B near the $\nu=5/2$ state, measured at the physical edge of sample. A well-quantized plateau with width of 500-600 G is observed, similar to previous samples(5). Note that, the 2-probe measurements include an extra contact resistance.

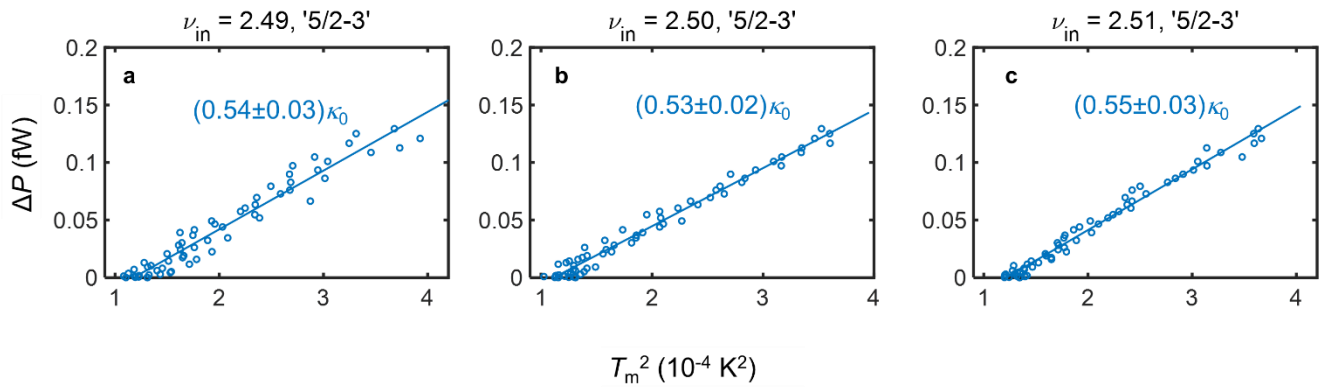


Figure S5 | '5/2-3' interface thermal conductance with different positions on the 5/2 plateau. The ΔP vs T_m^2 data for the '5/2-3' interfaces are plotted with a variation of the inner-gate filling ν_{in} on the 5/2 plateau. The extracted thermal conductances for these three positions are found to be $\sim 0.5\kappa_0$ (within the estimated error-bar).

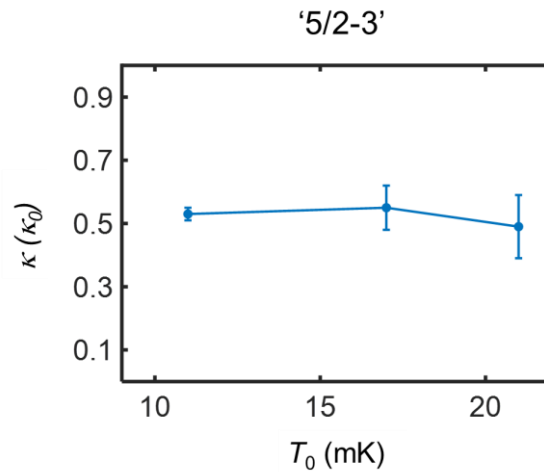


Figure S6 | Temperature dependence of the '5/2-3' interface Thermal conductance. The thermal conductance of '5/2-3' interface is plotted for three different base temperature $T_0 = 11, 17$ and 21 mK, and found to be almost constant within the estimated error-bars with $\kappa \approx 0.5\kappa_0$.